THESIS FOR THE DEGREE OF LICENTIATE OF ENGINEERING

Multiscale modeling of textile-reinforced concrete shells

GABRIEL EDEFORS

Department of Architecture and Civil Engineering
Division of Structural Engineering
CHALMERS UNIVERSITY OF TECHNOLOGY

Göteborg, Sweden 2025

Multiscale modeling of textile-reinforced concrete shells
GABRIEL EDEFORS

Thesis for the degree of Licentiate of Engineering
Technical report number: 2025:6

Department of Architecture and Civil Engineering
Division of Structural Engineering
Chalmers University of Technology
SE-412 96 Göteborg
Sweden
Telephone: +46 (0)31-772 1000

Cover:
The cover image depicts a single-curved textile-reinforced concrete shell together with the mesh of the large-scale model and a representative volume element located at one of its integration points.

Chalmers Reproservice
Göteborg, Sweden 2025

Multiscale modeling of textile-reinforced concrete shells

GABRIEL EDEFORS
Department of Architecture and Civil Engineering
Division of Structural Engineering
Chalmers University of Technology

Abstract

In textile-reinforced concrete (TRC), the steel bars of conventional reinforced concrete (RC) are replaced by non-corroding fiber textiles. Compared to RC, TRC requires less concrete cover, eliminates corrosion-related maintenance, and provides higher specific strength and stiffness.

Analyzing and designing TRC structures, however, is challenging due to the complex interaction between the yarns and the surrounding concrete, as well as the brittle behavior of the yarns. The latter limits the possibility for stress redistribution and, consequently, the applicability of plastic limit analysis. Most existing studies use smeared representations that capture average effects but sacrifice explicit access to subscale behavior. In contrast, computational homogenization averages the subscale response while maintaining a direct link between the scales. In this framework, calibration is only required at the subscale, making it independent of the structural geometry. Despite its computational cost, this approach facilitates accurate predictions of structural response while providing access to subscale quantities such as crack widths, crack spacing, and reinforcement stresses. Moreover, it opens the door to holistic optimization, where both structural parameters (e.g., topology and shape) and material-level features (e.g., concrete properties and reinforcement layout) can be optimized within a consistent framework.

Building on these considerations, the present work introduces a multiscale framework for the design and analysis of TRC shells. A two-scale shell model is derived from the single-scale problem using Variationally Consistent Homogenization (VCH) with Kirchhoff–Love kinematics. The subscale simulations are performed on Representative Volume Elements (RVEs), where the effect of partial yarn activation is captured using efficiency factors. A second-order expansion of the out-of-plane displacement is also shown to be required for kinematic consistency. While suitable for generating offline data, upscaling through computational homogenization is often too time-consuming for online simulations. To overcome this, a surrogate model acting directly at the sectional level was introduced for use in the online stage of structural analysis. This model is thermodynamically consistent, accounts for tensile and compressive damage, and can be trained on multiscale simulation data. Further, it generalized well beyond the training data, accurately predicting responses under cyclic loading. Compared with a fully resolved single-scale simulation of a one-way slab, the proposed approach achieved comparable numerical results while being two orders of magnitude faster.

Together, these contributions represent significant progress toward the long-term goal of a practical multiscale framework for the design and optimization of TRC shells. The framework balances accuracy and computational efficiency and lays the foundation for integration into multiscale optimization workflows.

Keywords: TRC, concrete, shell, damage modeling, computational homogenization

I knew exactly what to do.
But in a much more real sense, I had no idea what to do.

Preface

This work was carried out at the Department of Architecture and Civil Engineering and the Department of Industrial and Materials Science at Chalmers University of Technology between May 2023 and December 2025. The research was funded by the Swedish Research Council (Vetenskapsrådet) under grant no. 2022-03708. The computations were enabled by resources provided by Chalmers e-Commons at the Chalmers Center for Computational Science and Engineering (C3SE).

Acknowledgements

First and foremost, I would like to express my sincere gratitude to my supervisors, Prof. Karin Lundgren and Prof. Fredrik Larsson, as well as to my examiner, Prof. Leif Asp. You have been like workplace parents, guiding me through both joy and hardship with patience, wisdom, and encouragement. In particular, I wish to extend my heartfelt thanks to Fredrik for his constant willingness to engage in discussions on weak (and strong) forms over a good cup of coffee and to Karin for always being so supportive and positive. I truly look forward to the second half of this PhD game, and I hope we can score some meaningful research goals together.

I am also deeply grateful to my colleagues (and friends) for making these past years so fun. From the very first day, I have felt welcomed and appreciated at both departments, and it is truly unfortunate that I must divide my time between them. Special thanks go to my roommate and decoration partner, Caroline Ansin, for her invaluable advice, endless conversations, and generous willingness to lend me her charger. I'm convinced we've discussed nearly everything imaginable while still managing to get some work done, that's what I call productivity!

I also wish to thank Andreas Alhede, my desk neighbor and friend at structural engineering, for all the enjoyable moments we have shared and the help you have provided. If all mentors offered as much support as you have, I suspect supervisors might hardly be needed. It has also been easier to come to work after a Blåvitt loss knowing I could discuss the game with you.

Lastly, thanks to the designer (and fiancée) Olivia, for all her help with the illustrations and color schemes. The thesis *would still have been possible* without you, but the figures would definitely have looked worse.

Gothenburg, December 2025
Gabriel Edefors

Thesis

This thesis consists of an extended summary and the following appended papers:

Paper A G. Edefors, F. Larsson, and K. Lundgren, "Computational homogenization for predicting the effective response of planar textile-reinforced concrete shells". *International Journal of Solids and Structures*, **320** (2025), Article 113472. https://doi.org/10.1016/j.ijsolstr.2025.113472.

Paper B G. Edefors, F. Larsson, and K. Lundgren, "A Damage-Based Sectional Constitutive Model for Beams: Application to One-Way Textile-Reinforced Concrete Slabs". Manuscript.

The appended papers were prepared in collaboration with the co-authors. The author of this thesis carried the main responsibility for developing and implementing the models, performing the simulations, and drafting the manuscripts.

Contents

Part I
Extended Summary

1. Introduction

This chapter provides the background and motivation for the research, establishes the context for the thesis, and outlines the research aim, objectives, and scope.

1.1 Background and motivation

Cement-based composites such as concrete are by far the most widely used construction materials, with an annual production exceeding ten billion tons [1]. The cement industry alone accounts for approximately 6% of global CO_2 emissions [2]. Consequently, reducing emissions in the construction industry requires the development of alternative materials to conventional reinforced concrete (RC). One such material is textile-reinforced concrete (TRC), a cement-based composite in which the reinforcement consists of textiles, typically made of glass or carbon fibers. Structures made of TRC can be made thinner than RC, since the textiles are not susceptible to corrosion and therefore do not require a thick protective cover. The higher mass-specific strength of the reinforcement reduces the required reinforcement mass, which in turn lowers the self-weight of the structure [3]. Several studies have shown significant reductions in CO_2-equivalent emissions, despite the higher emission intensity per unit mass of both the concrete matrix and the reinforcement compared to RC. Reported examples include a pedestrian bridge with a 26% reduction and façade elements with a 30% reduction [4, 5]. Beyond these potential reductions in CO_2-equivalent emissions, the flexibility of textiles makes TRC well suited for curved structures, enabling designs that optimize load-transfer mechanisms. For instance, research indicates that if floors are constructed as thin concrete shells carrying loads primarily through membrane action, CO_2-equivalent emissions could be reduced by up to 65% [6].

Although TRC offers clear structural and environmental advantages, fully realizing its potential requires addressing modeling challenges arising from its complex material response. The yarns consist of hundreds to thousands of filaments, leading to complex interactions with the concrete matrix. Slip can occur both between the outer filaments and the concrete and within the yarn between outer and inner filaments [7]. Together with matrix cracking and crushing, these mechanisms produce a highly non-linear response. For design purposes, accurately characterizing this response is crucial, as the potential for stress redistribution is limited [8]. The most direct way to capture it would be to explicitly resolve all subscale features, including yarns and the surrounding matrix, throughout the entire structure. However, running large-scale simulations with such high fidelity is in practice infeasible due to the high computational cost [9]. As a compromise, semi-resolved models have been developed, where yarns are modeled explicitly, at varying

levels of geometric detail, while the concrete is treated as a continuum [10]. More recently, research has focused on model-reduction techniques that can replace these computationally demanding approaches. A prominent class of such methods is smeared models, in which the effect of the reinforcement is represented implicitly, either through phenomenological or mechanistic formulations. In these models, the cross-section is typically discretized into lamellae, each assigned its own material behavior. The lamella response can be described directly through phenomenological laws calibrated at the structural scale, as in [11], or through mechanistic approaches such as the microplane model proposed by Chudoba et al. [12, 13]. In the latter, the macroscopic stress and strain tensors are projected onto multiple microplanes, where the constitutive response is evaluated using local damage functions calibrated from experimental data.

In this work, the term subscale refers to the length scale at which the concrete matrix and the yarns are represented as distinct but homogeneous materials, similar to the use of mesoscale in [14]. The large scale, in contrast, refers to the length scale of the structural element, at which the overall behavior of the TRC member (e.g., plate or shell) is modeled.

Another important strategy for reducing computational complexity is multiscale modeling. In this approach, heterogeneities at smaller length scales are not resolved explicitly in the structural analysis but are instead represented through homogenization, ensuring consistency across scales [15]. The material-point response at the structural scale is then obtained by solving a subscale problem on a Representative Volume Element (RVE) and homogenizing the response. Computational homogenization has been applied to RC plates [16] and TRC elements [9], but to the author's knowledge, not yet to TRC shells. Analytical homogenization has been used for continuum representations of TRC [17] and in multiscale frameworks [18], while a related hybrid stress-resultant homogenization was proposed for RC membranes by Huguet et al. [19].

Applying computational homogenization to TRC shells provides a consistent framework for capturing important mechanisms such as bond-slip, cracking, and crushing without explicitly resolving all subscale features. This approach enables accurate predictions of stress redistribution, deflections, and ultimate capacity at a lower computational cost than a fully resolved simulation, while also facilitating holistic multiscale optimization.

Typically, computational homogenization is implemented in a nested concurrent fashion, for instance through the Finite Element Squared (FE^2) method, in which each integration point of the structural model is coupled to an RVE. While $\mathbf{FE^2}$ provides a rigorous scale-bridging framework, it is also computationally demanding, as it requires solving a boundary value problem at every integration point and for each large-scale iteration [20]. To mitigate the computational cost in practical implementations, significant effort has been devoted to developing surrogate models that replace the homogenization step, for instance through machine learning approaches as in [21, 22] or physics-based models with reduced parameter sets, as in [23]. A common characteristic of these methods is their reliance on homogenization-based upscaling to generate training data for calibrating the surrogate, either prior to the simulation (offline stage) or dynamically during the simulation (online stage).

1.2 Research aim and objectives

Against this background, the goal of the PhD project is to develop a multiscale modeling framework for TRC shells that combines accuracy and computational efficiency, and that can be applied to both structural analysis and design optimization. As an intermediate step towards this goal, the current work addresses the following objectives:

1. To apply computational homogenization to derive an upscaling model for TRC shells that accounts for subscale heterogeneities and interactions, ensuring a consistent transition between fully resolved and effective representations. This objective is achieved through the following steps:
   (a) To establish a two-scale model for TRC shells based on Kirchhoff–Love kinematics.
   (b) To implement the subscale RVE problem to enable simulation of the effective shell response.
   (c) To validate the two-scale model against a fully resolved single-scale TRC model.

2. To develop a surrogate model that provides reliable predictions during the online stage at significantly reduced computational cost. This objective includes:
   (a) To establish a thermodynamically consistent constitutive model acting directly at the sectional level, linking generalized strains and stresses.
   (b) To calibrate and validate the surrogate model using data obtained from the upscaling framework.

1.3 Scope and limitations

This work builds on the single-scale problem, in which the interaction between the yarns and the concrete is modeled using the approach proposed by Sciegaj et al. [24] and validated experimentally in [25]. The model captures the non-uniform stress distribution within the yarns through efficiency factors. While this representation captures the overall effect on the large-scale response, explicitly resolving the filaments would be required to accurately capture effects related to confinement pressure or progressive failure. The upscaling into an effective shell model is performed using variationally consistent homogenization (VCH). This ensures energetic consistency between scales and provides a systematic way to derive both the sub- and large-scale problems as well as the scale transition between them. At the subscale, the initial curvature of the shell is neglected. Curved shell structures could nevertheless be modeled within this framework by representing the geometry with flat facet elements in the large-scale model. Furthermore, localization is considered at the subscale but not at the large scale, since localization is a subscale phenomenon in adequately reinforced TRC structures. To address computational cost, the surrogate constitutive model in this thesis is formulated for one-way members such as beams, as a first step toward extension to general plates and shells. The multiscale framework in this work is validated against direct numerical simulations, so its accuracy

is assessed relative to the single-scale model.

2. Textile-reinforced concrete

The following chapter introduces the fundamental aspects of textile-reinforced concrete, focusing on its composition and mechanical behavior, and establishes the foundation for the modeling work presented later in the thesis.

2.1 Composition

Textile-reinforced concrete (TRC) consists of a fine-grained concrete matrix reinforced with textiles, see Figure 2.1. The textiles can be woven or knitted, with the plain weave being the simplest configuration. They consist of yarns made of inorganic fiber filaments, most commonly carbon or alkali-resistant glass [26]. They can either be planar and aligned with the principal stress directions (similar to steel bars in RC) or three-dimensional to provide strength and stiffness in multiple directions [27]. Compared to steel reinforcement, the smaller perimeter and closer spacing of the yarns result in finer crack patterns and smaller crack widths [28, 29]. Unlike steel bars in reinforced concrete (RC), where the strain distribution is essentially uniform, the stress in a textile yarn is highly non-uniform because only the outer filaments are in direct contact with the matrix. Stress transfer to the inner filaments depends on friction and cohesion, leading to interfilament slip and partial activation of the yarn cross-section [30]. This drawback can be mitigated by impregnating the yarns, which improves internal stress transfer and enhances load-bearing capacity [31]. To capture this behavior, some authors model the yarns as segmented elements (e.g., layers, sectors, or laminae) and characterize the stress transfer between them, while others employ more phenomenological models, in which the effective stress–strain response or stiffness is represented through efficiency factors derived directly from pull-out tests [24, 32, 33, 31]; see Figure 2.2.

2.2 Mechanical response

The composite response of TRC is governed by many factors such as the stiffness and strength of the yarns, the degree of activation of the yarns, the slip between the yarns and the matrix and the tensile and compressive strength of the concrete. Starting with the yarns, a common approximation is that they behave linearly elastically up to failure. At the onset of loading in tension, a delayed activation is typically observed, caused by the straightening of the yarns [34]. The concrete behaves approximately linearly elastically up to its tensile strength, after which microcracks form and gradually coalesce

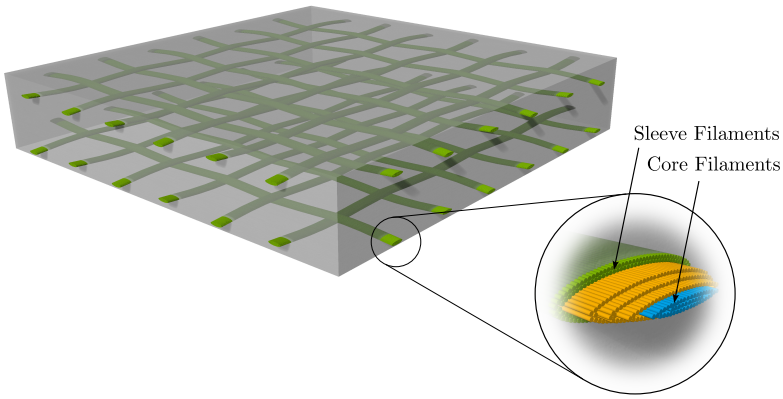

Figure 2.1: *Cut-out of a textile reinforced shell with plain weave reinforcement placed along the top and bottom faces. The zoom-in shows how the yarn is made up of smaller filaments.*

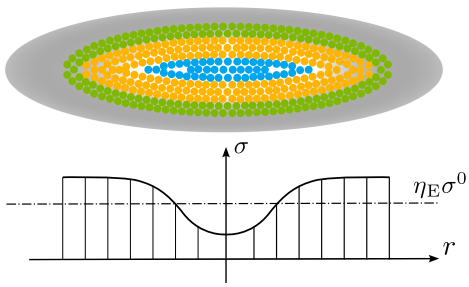

Figure 2.2: *Illustration of the non-uniform stress distribution in a yarn, and its approximation by a uniform stress state. The uniform effective stress can be expressed in terms of the nominal stress (assuming equal strain in all filaments) σ^0 and a stiffness efficiency factor η_{E}.*

into a fracture zone (macrocrack). In this fracture zone, the stress decreases and the deformation increases [35]. Concrete also exhibits compressive damage (crushing), albeit at much higher stress levels, with compressive strength typically about ten times the tensile strength [36]. This failure mode is more diffuse than the localized cracks in tension and is typically characterized by microcracking parallel to the principal loading direction (axial splitting cracks) and by shear deformations developing within inclined shear bands [37, 38].

Together, the concrete matrix and the textile reinforcement form a strain-hardening composite, whose characteristic uniaxial tensile response is illustrated in Figure 2.3. At small strains, the response is linear-elastic and governed primarily by the concrete. Once the tensile stress reaches a critical value, microcracks coalesce into the first macrocrack, typically at a transverse yarn, causing a sudden reduction in stiffness [39]. At the crack plane, the tensile load is carried entirely by the yarns, while away from the crack it is gradually transferred back to the concrete matrix through bond stresses. At a certain distance from the crack, the tensile stress in the matrix reaches its tensile strength and a new crack forms. This process repeats until the bond transfer is no longer sufficient to initiate additional cracks, marking the end of the multiple-cracking stage. Beyond this stage, further strain is accommodated mainly by yarn deformation rather than additional bond-slip, leading to a gradual stiffening that asymptotically approaches that of the reinforcement. Since not all filaments within a yarn are fully activated (see Figure 2.2), the stiffness does not reach that of the plain textiles, necessitating the use of an effective stiffness [24]. Ultimately, tensile failure in TRC occurs either through yarn rupture, telescopic pull-out of the inner filaments, or a combination of both [40], and typically develops without the pronounced plastic deformations characteristic of conventional reinforced concrete. If the yarns have insufficient anchorage the composite may also fail in so called anchorage failure where the whole yarns are simply pulled out of the concrete [41]. Whereas tensile failure is governed by the yarns and their interaction with the concrete, the compressive strength of the concrete can be decisive in compression or bending, depending on the reinforcement ratio [42].

From a modeling perspective, several approaches exist to capture the nonlinear behavior described above. The combined effects of cracking and crushing can be represented using damage–plasticity formulations, originally proposed by Lubliner et al. [43] and later extended to more general loading conditions, e.g. [44, 45]. Although pure damage models reproduce the dominant response under cracking and compressive softening, experimental investigations have shown that TRC can also exhibit plastic behavior [46, 47], arising from residual bond slip, plasticity of the concrete in compression, and incomplete crack closure [48, 34]. In this thesis, however, a simplified representation is adopted: both cracking and crushing of the concrete are modeled using a pure damage formulation as done in e.g. [49, 50]. While this comes with certain limitations, it provides a consistent and computationally efficient modeling framework for the multiscale framework.

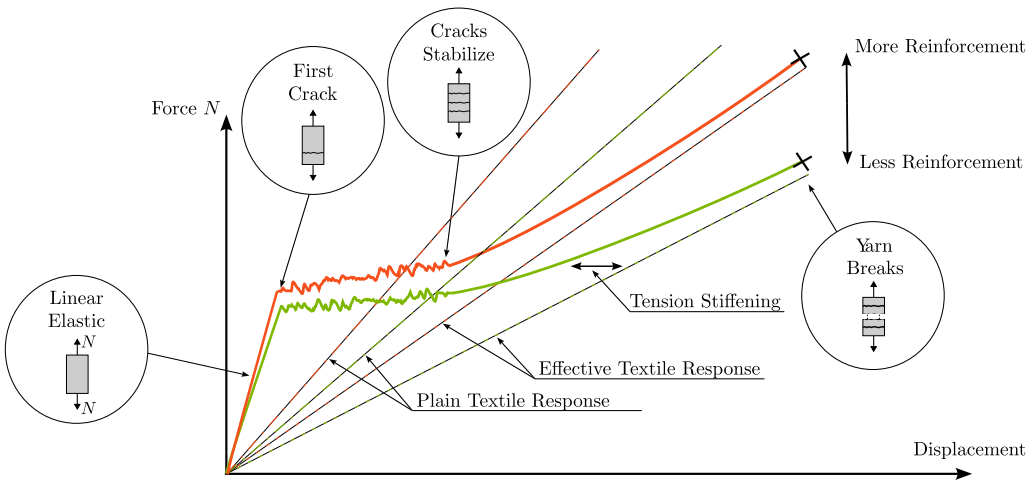

Figure 2.3: *Schematic graph of a typical force-displacement relation for different amounts of reinforcement.*

3. Upscaling of textile-reinforced concrete

This chapter introduces the general concepts of multiscale modeling and outlines the method adopted in this work. It also presents surrogate constitutive modeling, with particular emphasis on damage mechanics as the underlying framework.

3.1 Multiscale modeling

Multiscale modeling is a broad class of methods for analyzing materials across different length and time scales. Such approaches are particularly valuable when the subscale exhibits complex heterogeneity that influences the structural response. Since resolving these features directly at the large scale is computationally expensive [20], multiscale methods provide an efficient alternative.

Two main categories are typically distinguished: hierarchical (or sequential) and concurrent (or nested) approaches. In hierarchical approaches, information flows only from finer to coarser scales: effective properties are derived in an offline stage and then used at the coarser scales without coupling the scales [51]. Examples of applications to TRC include [14, 18]. In contrast, concurrent methods feature two-way coupling: fine-scale and coarse-scale boundary value problems are solved together, with the solution on one scale providing input to the other. In practice, concurrent methods are often implemented via the FE^2 method, where subscale simulations are embedded directly in the integration points of the large-scale model [52].

A particularly important family of multiscale methods employs homogenization to bridge the scales. Homogenization may rely on analytical schemes (e.g., Voigt, Reuss) [53], asymptotic expansions [54], or numerical techniques (computational homogenization) [15]. In all cases, the essential idea is to derive an effective response at the coarse scale from the fine-scale behavior, ensuring consistency between the two descriptions [55]. The transition from the finer to the coarser scale is performed through homogenization, where the homogenization operator provides the mapping between scales. In a continuum setting, this operator, denoted by $\langle\cdot\rangle_\square$, is typically defined as the volume average of a subscale field over the RVE $\Omega_\square$, i.e.

$$\langle\,\cdot\,\rangle_\square = \frac{1}{|\Omega_\square|}\int_{\Omega_\square}(\cdot)\,\mathrm{d}V. \tag{3.1}$$

The homogenization procedure may, however, take different forms, provided that it sat-

isfies the Hill–Mandel macro-homogeneity condition, which ensures energetic equivalence between the subscale and macroscale virtual work. In the general continuum setting this reads

$$\begin{aligned} \langle \boldsymbol{\sigma} : \delta\boldsymbol{\varepsilon} \rangle_{\square} &= \bar{\boldsymbol{\sigma}} : \delta\bar{\boldsymbol{\varepsilon}}, \\ \bar{\boldsymbol{\sigma}} &= \langle \boldsymbol{\sigma} \rangle_{\square}, \\ \bar{\boldsymbol{\varepsilon}} &= \langle \boldsymbol{\varepsilon} \rangle_{\square}. \end{aligned} \tag{3.2}$$

In computational homogenization, the core idea is to subject a representative part of the substructure to large-scale loading and evaluate the corresponding effective response though homogenization. The smallest subvolume for which the effective parameters converge is called the representative volume element (RVE). For periodic substructures, as is often the case in TRC, the unit cell with periodic boundary conditions constitutes an RVE in the linear elastic regime [15]. Once damage localizes and bond slip develops, periodicity no longer holds, and the RVE must be enlarged to ensure convergence.

Validity of homogenization further requires a clear separation of scales: the characteristic length of the periodicity must be much smaller than the structural length scale, so that the large-scale fields can be regarded as smooth across the RVE [15]. If this condition is violated, truncating the large-scale fields (typically up to the linear terms) within the RVE problem is no longer a valid approximation.

Applications of homogenization to TRC include computational approaches [9] and analytical schemes [17]. Computational homogenization has also been applied to plates and shells, where homogenization is typically carried out in-plane, while the through-thickness variation is represented using plate kinematics. Depending on the formulation, this may involve Kirchhoff-Love kinematical assumptions [16, 56, 57] or Reissner–Mindlin kinematical assumptions [58, 59, 60].

3.2 Variationally Consistent Homogenization

A systematic framework for deriving the coupled boundary value problems of the sub- and large-scale is provided by Variationally Consistent Homogenization (VCH) [61]. The procedure starts from the weak form of the single-scale boundary value problem. The displacement field is additively decomposed into a fluctuating subscale component, $\boldsymbol{u}^{\mathrm{s}}$, and a prolonged large-scale component, $\boldsymbol{u}^{\mathrm{L}}$, i.e.

$$\boldsymbol{u} = \boldsymbol{u}^{\mathrm{s}} + \boldsymbol{u}^{\mathrm{L}}. \tag{3.3}$$

In first-order homogenization the large-scale fields are prolonged using a first-order Taylor expansion. Consequently, if displacement is the primary field, the associated large-scale contribution to the strain is constant on the subscale. When this assumption no longer holds, for instance in the presence of pronounced strain gradients, higher-order homogenization schemes can be employed, as proposed in [62]. For the upscaling of planar shells in this thesis, the through-thickness displacement field is assumed to follow the Kirchhoff–Love kinematic assumptions. This implies that the in-plane displacement field can be parameterized by the large-scale mid-plane displacement vector $\bar{\boldsymbol{u}}_{\mathrm{p}}$ and the large-scale transverse displacement $\bar{w}$, such that

$$\boldsymbol{u}_{\mathrm{p}}\left(\bar{\boldsymbol{x}}_{\mathrm{p}}, z\right) = \bar{\boldsymbol{u}}_{\mathrm{p}} - z\boldsymbol{\nabla}_{\mathrm{p}}\bar{w}\big|_{\bar{\boldsymbol{x}}_{\mathrm{p}}} . \tag{3.4}$$

The in-plane displacement field is prolonged using a first-order Taylor expansion, whereas the out-of-plane displacement field must be prolonged using a second-order Taylor expansion to remain consistent with the Kirchhoff–Love assumption and thereby avoid over-constraining the RVE. For clarity, the prolongation is illustrated in Figure 3.1 for the one-dimensional case of a beam subjected to pure bending ($\bar{u}(\bar{x}) = 0$), evaluated at a large-scale point at mid-span ($\bar{\theta} = 0$).

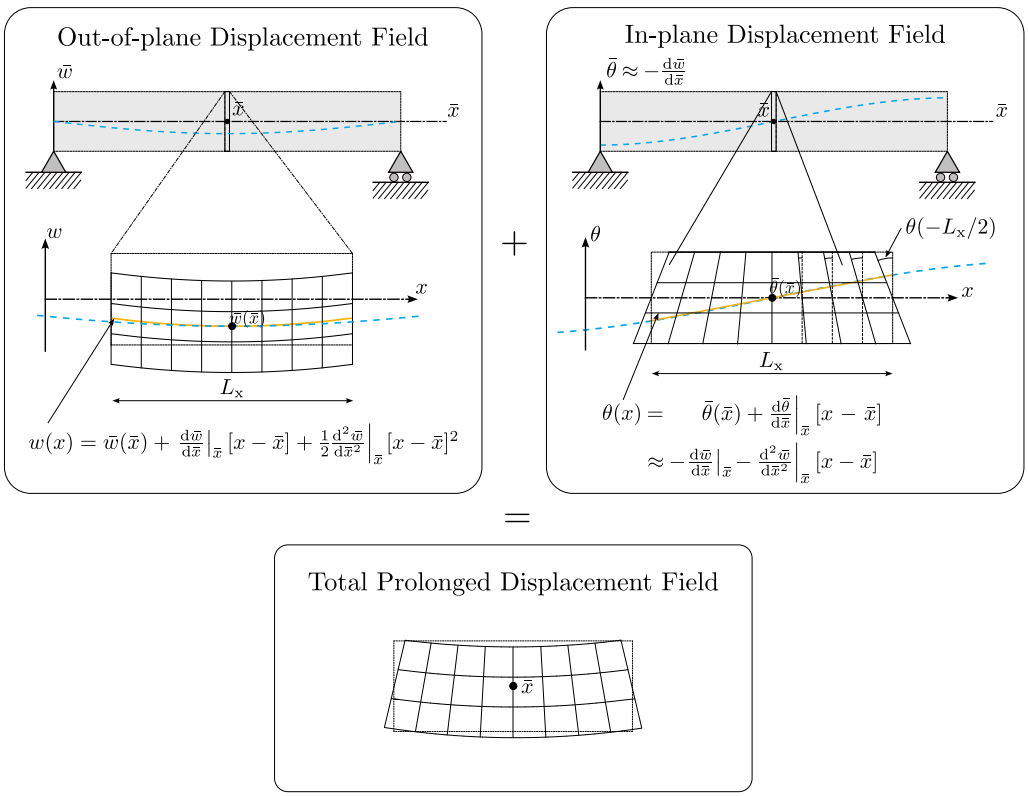

Figure 3.1: *Prolongation of the displacement fields in a beam for the case of pure bending. To the left is the prolongation of the out-of-plane displacement components and to the right is the prolongation of the axial displacement component. In the bottom is the total prolonged displacement field obtained as a superposition of the two fields.*

The next step is to approximate the fields by running averages over a window corresponding to the RVE. Localizing the problem to the RVE and testing with functions associated with the fluctuating subscale fields yields the boundary value problem for the RVE. To make this problem well-posed, the boundary conditions must be consistent with the Hill-Mandel conditions stated in Equation 3.2. Three standard choices that fulfill this

are:

- **Dirichlet (uniform displacement):** the large-scale part of the displacement field is directly prescribed on the RVE boundary. Gives an *upper bound* on the response.
- **Neumann (uniform traction):** the large-scale part of the displacement field is imposed on the RVE such that the resulting boundary traction corresponds to constant effective (large-scale) stress. For the shell, this means that the membrane stress and moments act as constant Lagrange multipliers. Gives a *lower bound* on the response.
- **Periodic:** opposite RVE faces are constrained to have periodic displacements and anti-periodic tractions. For periodic microstructures, this choice is typically the most accurate.

Similarly, the large-scale problem is obtained by testing with functions pertaining to the prolonged primary large-scale fields. The structure of the large-scale problem directly determines the homogenization expressions for the effective fields, defined as the energetic conjugates of the large-scale primary variables. The homogenization operator, here taken as the averaging operator $\langle\cdot\rangle_\square$ introduced in Equation 3.1, must be consistent with the chosen prolongation ansatz. In other words, the average of a prolonged large-scale field should reproduce the large-scale quantity itself.

3.3 Surrogate constitutive model

A surrogate constitutive model serves as an efficient alternative to the upscaling step in computational homogenization. Instead of solving a boundary value problem at every integration point, as required in nested FE^2 simulations, the surrogate provides a direct constitutive relation at the large scale. This enables the effective sectional response to be evaluated at a fraction of the computational cost, while retaining the essential physics, most importantly thermodynamic consistency, captured by the detailed RVE simulations.

Conceptually, the surrogate model represents a fictitious effective cross-section characterized by a reduced set of parameters compared to the RVE. These parameters are calibrated using data obtained from the VCH framework introduced earlier, ensuring that the surrogate approximates the macroscopic response of the detailed multiscale model as closely as possible within its simplified formulation. Once calibrated, the surrogate model can be used in an online stage to predict the stress–resultant response under arbitrary combinations of membrane strain and curvature histories.

The surrogate formulation is based on continuum damage mechanics, which provides a thermodynamically consistent description of stiffness degradation due to cracking and crushing. In the following, this damage framework is introduced, followed by its extension to the sectional level.

3.3.1 Continuum damage model

Constitutive models are typically formulated within a thermodynamic setting. The starting point is the second law of thermodynamics, or more specifically the Clausius–Duhem

inequality. Under isothermal conditions and invoking the energy balance (first law), this reduces to the dissipation inequality

$$\mathcal{D} = \boldsymbol{\sigma} : \dot{\boldsymbol{\varepsilon}} - \dot{\Psi} \quad \geq 0, \tag{3.5}$$

where $\Psi = \rho e - \rho T s$ is the Helmholtz free energy per unit volume, representing the recoverable part of the internal energy [63]. The Helmholtz free energy is typically expressed in terms of the strain $\boldsymbol{\varepsilon}$ and internal variables $\boldsymbol{a}$ that capture history effects, i.e. $\Psi = \Psi(\boldsymbol{\varepsilon}, \boldsymbol{a})$. In plasticity, internal variables typically characterize the evolution of the yield surface, whereas in damage mechanics they quantify the progressive degradation of the material stiffness. For isothermal linear elasticity, the Helmholtz free energy takes the quadratic form

$$\Psi^0(\boldsymbol{\varepsilon}) = \tfrac{1}{2}\, \boldsymbol{\varepsilon} : \boldsymbol{C} : \boldsymbol{\varepsilon}. \tag{3.6}$$

The dissipation inequality in Equation (3.5) is then satisfied for arbitrary strain paths if the stress is defined as the energy conjugate to the strain,

$$\boldsymbol{\sigma} = \frac{\partial \Psi^0}{\partial \boldsymbol{\varepsilon}}. \tag{3.7}$$

In isotropic damage mechanics, the state of degradation is represented by a single internal variable $d \in [0, 1]$. This degradation is applied directly to the Helmholtz free energy [64, 65],

$$\Psi(\boldsymbol{\varepsilon}, d) = (1 - d)\Psi^0(\boldsymbol{\varepsilon}), \tag{3.8}$$

which leads to the degraded stress response

$$\boldsymbol{\sigma} = \frac{\partial \Psi(\boldsymbol{\varepsilon}, d)}{\partial \boldsymbol{\varepsilon}} = (1 - d)\, \boldsymbol{\sigma}^0, \tag{3.9}$$

where $\boldsymbol{\sigma}^0 = \boldsymbol{C} : \boldsymbol{\varepsilon}$ denotes the effective stress. Thus, the tangent stiffness decreases with increasing d, resulting in strain softening. The energy release rate conjugate to d is

$$Y = -\frac{\partial \Psi(\boldsymbol{\varepsilon}, d)}{\partial d} = \Psi^0(\boldsymbol{\varepsilon}), \tag{3.10}$$

showing that, at fixed strain, the driving force for damage growth equals the undamaged free energy $\Psi^0(\boldsymbol{\varepsilon})$ and therefore grows quadratically with strain. Substituting Equation (3.8) and Equation (3.9) into the general inequality in Equation (3.5) gives

$$\mathcal{D} = Y\, \dot{d} \quad \geq 0, \tag{3.11}$$

which is satisfied by enforcing the irreversibility condition $\dot{d} \geq 0$ (with $\dot{d} = 0$ during unloading) together with the non-negative form of the effective strain energy density Ψ^0 in Equation 3.6.

In practice, the irreversibility condition is enforced by introducing a history variable α, defined as the maximum attained value of the damage-driving variable Y,

$$\alpha(t) = \max_{\tau \in [0,t]} Y(\tau), \tag{3.12}$$

which guarantees that $\dot{\alpha} \geq 0$, and thus $\dot{d} \geq 0$ for any monotonic damage law $d(\alpha)$. Together with the requirement that damage should not initiate before a threshold k, this constrains the admissible form of the damage evolution function. A convenient choice is the exponential law

$$d(\alpha) = \begin{cases} 0, & \alpha < k, \\ D_{\max}\left[1 - \exp\left(-\dfrac{\alpha - k}{\beta}\right)\right], & \alpha \geq k, \end{cases} \tag{3.13}$$

where $D_{\max}$ is the damage cap, β controls the shape of the exponential function, and k is the damage threshold. The resulting uniaxial stress-strain response in tension is illustrated in Figure 3.2.

3.3.2 Sectional damage model

Starting from the general case of a Kirchhoff-Love shell, the local strain is described by the generalized strains: the membrane strain $\bar{\boldsymbol{\varepsilon}}$ and the curvature $\bar{\boldsymbol{\kappa}}$, such that $\boldsymbol{\varepsilon}(z) = \bar{\boldsymbol{\varepsilon}} - z\bar{\boldsymbol{\kappa}}$. The free energy density per unit mid-plane area of the shell is obtained by integrating the free energy density in Equation 3.6 through the thickness, yielding

$$\bar{\Psi} = \tfrac{1}{2}\,\bar{\boldsymbol{\varepsilon}} : \underbrace{\left(\int_{-h/2}^{h/2} \boldsymbol{C}(z)\,\mathrm{d}z\right)}_{\bar{\boldsymbol{C}}_{\mathrm{h}}} : \bar{\boldsymbol{\varepsilon}} - \bar{\boldsymbol{\varepsilon}} : \underbrace{\left(\int_{-h/2}^{h/2} z\,\boldsymbol{C}(z)\,\mathrm{d}z\right)}_{\bar{\boldsymbol{C}}_{\mathrm{S}}} : \bar{\boldsymbol{\kappa}} + \tfrac{1}{2}\,\bar{\boldsymbol{\kappa}} : \underbrace{\left(\int_{-h/2}^{h/2} z^2\,\boldsymbol{C}(z)\,\mathrm{d}z\right)}_{\bar{\boldsymbol{C}}_{\mathrm{I}}} : \bar{\boldsymbol{\kappa}}. \tag{3.14}$$

For the simplest case, $\boldsymbol{C}(z)$ denotes the plane-stress isotropic stiffness tensor representing the material stiffness at position z through the thickness of the effective cross section. Under uniaxial response, and accounting for damage through the set of (piecewise constant in the section) damage variables $\bar{\boldsymbol{d}}$, this expression reduces to

$$\bar{\Psi}(\bar{\varepsilon}, \bar{\kappa}, \bar{\boldsymbol{d}}) = \tfrac{1}{2}\bar{C}_{\mathrm{A}}(\bar{\varepsilon}, \bar{\kappa}, \bar{\boldsymbol{d}})\,\bar{\varepsilon}^2 - \bar{C}_{\mathrm{S}}(\bar{\varepsilon}, \bar{\kappa}, \bar{\boldsymbol{d}})\,\bar{\varepsilon}\bar{\kappa} + \tfrac{1}{2}\bar{C}_{\mathrm{I}}(\bar{\varepsilon}, \bar{\kappa}, \bar{\boldsymbol{d}})\,\bar{\kappa}^2, \tag{3.15}$$

where the generalized sectional stiffness coefficients are given by

$$\bar{C}_{\mathrm{A}}(\bar{\varepsilon}, \bar{\kappa}, \bar{\boldsymbol{d}}) = \int_{-h/2}^{h/2} C(z)\,\zeta(z; \bar{\varepsilon}, \bar{\kappa}, \bar{\boldsymbol{d}})\,\mathrm{d}z, \tag{3.16a}$$

$$\bar{C}_{\mathrm{S}}(\bar{\varepsilon}, \bar{\kappa}, \bar{\boldsymbol{d}}) = \int_{-h/2}^{h/2} C(z)\,z\,\zeta(z; \bar{\varepsilon}, \bar{\kappa}, \bar{\boldsymbol{d}})\,\mathrm{d}z, \tag{3.16b}$$

$$\bar{C}_{\mathrm{I}}(\bar{\varepsilon}, \bar{\kappa}, \bar{\boldsymbol{d}}) = \int_{-h/2}^{h/2} C(z)\,z^2\,\zeta(z; \bar{\varepsilon}, \bar{\kappa}, \bar{\boldsymbol{d}})\,\mathrm{d}z. \tag{3.16c}$$

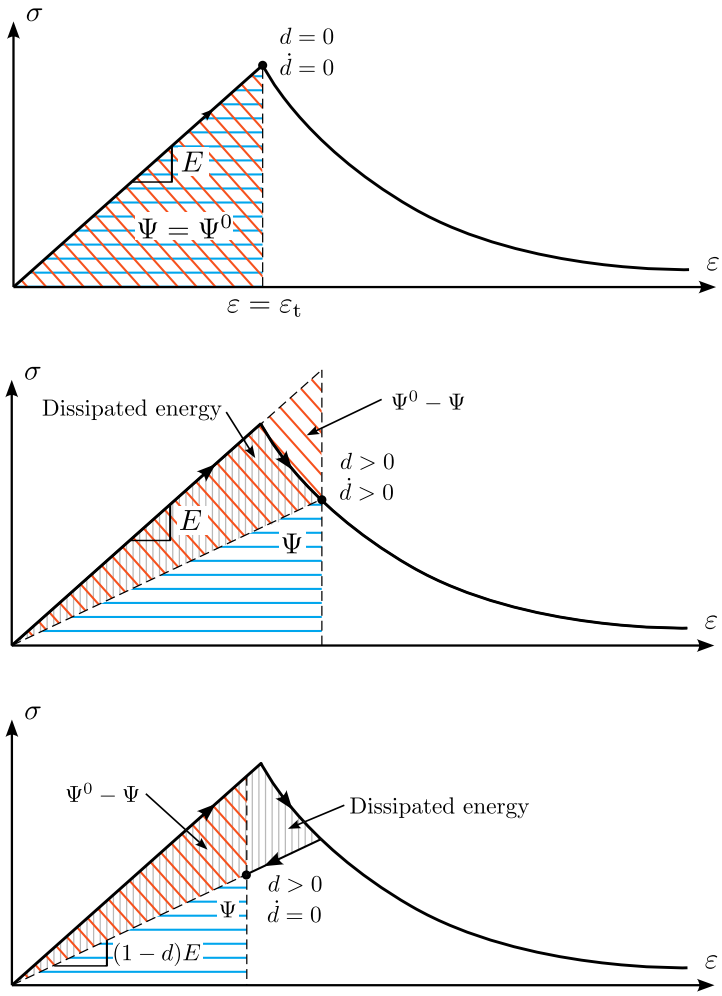

Figure 3.2: *Partition of the free energy during elastic loading (top), during damage growth (middle), and unloading (bottom). The blue region corresponds to the recoverable elastic energy Ψ, the red region corresponds to the difference between the undamaged free energy and the recoverable free energy $\Psi^0 - \Psi$ and the black region corresponds to the total energy dissipation.*

Here, $C(z) = E(z)$ represents the Young's modulus for a beam ($\sigma_{22} = \sigma_{12} = 0$), or $C(z) = E(z)/(1-\nu(z)^2)$ for a transversely constrained one-way slab ($\varepsilon_{22} = \varepsilon_{12} = 0$). The term $E(z)/(1-\nu(z)^2)$ can thus be interpreted as a scaling factor accounting for the Poisson effect. Importantly, both cases can be represented by a scalar stiffness coefficient, which keeps the model structure identical. The function ζ acts as a damage activation function activating the correct damage function depending on the local strain state (tensile or compressive). In this work, separate damage variables are assigned to the upper and lower parts of the section, following the approach in [66]. In this work $\bar{\boldsymbol{d}} = (d_{\mathrm{u}}^{\mathrm{t}}, d_{\mathrm{l}}^{\mathrm{t}}, d_{\mathrm{u}}^{\mathrm{c}}, d_{\mathrm{l}}^{\mathrm{c}})$, where the scalar damage variables $d_{\mathrm{u/l}}^{\mathrm{t/c}}$ corresponds to (t)ensile/(c)ompressive damage in the (u)pper/(l)ower part of the cross section.

The energy conjugates of the generalized strains are the normal force and bending moment, derived from the free energy density according to

$$\bar{N} = \left.\frac{\partial \bar{\Psi}}{\partial \bar{\varepsilon}}\right|_{\bar{\kappa},\bar{\boldsymbol{d}}} = \bar{C}_{\mathrm{A}}(\bar{\varepsilon},\bar{\kappa},\bar{\boldsymbol{d}})\bar{\varepsilon} - \bar{C}_{\mathrm{S}}(\bar{\varepsilon},\bar{\kappa},\bar{\boldsymbol{d}})\bar{\kappa}, \tag{3.17a}$$

$$\bar{M} = \left.\frac{\partial \bar{\Psi}}{\partial \bar{\kappa}}\right|_{\bar{\varepsilon},\bar{\boldsymbol{d}}} = \bar{C}_{\mathrm{I}}(\bar{\varepsilon},\bar{\kappa},\bar{\boldsymbol{d}})\bar{\kappa} - \bar{C}_{\mathrm{S}}(\bar{\varepsilon},\bar{\kappa},\bar{\boldsymbol{d}})\bar{\varepsilon}. \tag{3.17b}$$

4. Summary of appended papers

A short summary of the two appended papers is provided in this chapter.

Paper A

Paper A establishes the foundation for the multiscale analysis of TRC shells using computational homogenization. The starting point is a detailed single-scale model in which the yarns and their interaction with the concrete matrix are explicitly represented. The degradation of the concrete matrix is described with Mazars' damage model, enabling the prediction of tensile cracking and compressive softening. Based on this fine-scale description, variationally consistent homogenization is employed to derive both the weak form of the large-scale planar shell problem and the associated subscale RVE problem, together with the operators linking the two scales. A key novelty of this work is the identification of the need for a second-order prolongation of the vertical displacement field to prevent over-constraining the RVE in bending. The RVE serves as a virtual laboratory to quantify the effective response in terms of membrane forces and bending moments for prescribed large-scale strains and curvatures. The framework is validated against fully resolved direct numerical simulations of one- and two-way slabs, showing convergence of the effective stresses with increasing RVE size. Finally, the study demonstrates that the approach can predict effective responses for a variety of subscale and structural configurations without recalibration.

Paper B

While the multiscale framework in **Paper A** provides a virtual laboratory for design verification, its direct use in iterative design or optimization is somewhat limited by the high computational cost. To address this limitation, **Paper B** introduces a surrogate model for the analysis of unidirectional TRC members such as beams and one-way slabs. The model is formulated at the cross-section level as an effective constitutive relation, linking generalized strains (average strain and curvature) to generalized stresses (normal force and bending moment). The model accounts for both tensile and compressive damage, with separate sets of damage variables assigned to the upper and lower parts of the cross section. By working with the total strain field, the formulation naturally accounts for the combined effects of membrane strain and curvature. Thermodynamic consistency is ensured by verifying that the total energy dissipation remains non-negative. Calibration and validation are performed using data from distinct datasets obtained through RVE simulations. The surrogate model accurately predicts the response under several loading modes, including cyclic loading. It also enables an offline post-processing step, where the RVE can be used to study the detailed subscale response. Finally, the efficiency of the approach is demonstrated for a one-way slab with fixed ends, achieving nearly two orders of magnitude speed-up compared to a fully resolved simulation, with a maximum relative error below 12 %.

5. Conclusions and outlook

The following provides the main conclusions of the work and an outline of possible directions for further development of the modeling framework.

5.1 Summary of results and conclusions

The work presented in this thesis concerns multiscale modeling of TRC shells, with emphasis on predicting the effective shell response. In **Paper A**, the overall scale-bridging framework was developed, and it was shown that this can be used as a virtual laboratory to assess the large-scale response for varying subscale configurations. A key advantage of the framework is that it requires calibration only once for a given concrete–yarn combination, regardless of the reinforcement layout or section height. It was also demonstrated that the framework can provide accurate predictions as long as the separation of scales is sufficient and the RVE is sufficiently large. The relative error compared with direct numerical simulations of a one-way TRC slab was below 10% for cases with adequate scale separation at low to moderate membrane stress and up to 20% for high membrane stress (around 50% of the maximum bending stress). Moreover, three different boundary conditions were proposed: Neumann conditions to obtain a lower bound, Dirichlet conditions for an upper bound, and periodic conditions for the most accurate prediction.

The upscaling framework is designed to be flexible with respect to the choice of subscale model, allowing more refined constitutive descriptions for the concrete or yarns to be incorporated without modification of the overall framework. In particular, the framework enables a more detailed representation of the yarns, which can also be explicitly resolved if desired.

Although the computational homogenization framework provides a complete and consistent means of scale bridging, a more computationally efficient model is required for real-time concurrent simulations and optimization applications. Hence, in **Paper B**, a surrogate constitutive model was developed to replace costly RVE simulations. The model was calibrated using synthetic data obtained from RVE simulations and reproduced the response well for loading cases not included in the calibration, with an overall relative error of approximately 5–8%. It performed particularly well for loading scenarios with combined compressive membrane strain and bending, making it suitable for curved beams and one-way shells. Furthermore, the model reduced the computational cost by a factor of approximately 100 for a one-way TRC slab, while maintaining a maximum relative error of 12% compared to a fully resolved simulation. The nonlinear behavior is represented through a damage formulation, which makes the model especially suitable for TRC, where

the nonlinearity primarily arises from matrix degradation and bond–slip [12]. At present, the surrogate model is applicable to beam-type elements, for which closed-form solutions can be derived for the specific case of a homogeneous, rectangular effective cross-section, making the model computationally efficient.

5.2 Future work

The work carried out in this thesis provides a foundation for the multiscale modeling of TRC shells, but several aspects remain to be addressed in future research. These include generalizing the surrogate model to shell structures and extending it so that it can predict the response for varying section heights and reinforcement configurations, without the need for recalibration for each case. This would be required to fully replace the computational homogenization framework. In addition, the concrete damage model used in the RVE simulations was deliberately kept simple to highlight the generality of the approach. A more advanced formulation could, however, be incorporated within the same multiscale framework if a more accurate representation of compressive failure is desired. For the homogenization framework, the aspect of anchorage remains an open issue, since slip is currently treated as a locally varying field within the RVE. This prevents the model from capturing the progressive build-up of bond stress that develops over a finite distance in the large-scale domain. Possible approaches to address this limitation include enriching the two-scale model with a large-scale slip field as in [67] or introducing an efficiency factor that reduces the capacity near the ends to account for incomplete anchorage.

Finally, the two-scale formulation provides a natural foundation for optimization across scales, enabling the framework to be used not only for prediction but also for design. One possible direction is to optimize the subscale for a given large-scale configuration, similar to point-to-point material design [68]. A more general, but also considerably more demanding, approach would be full two-scale topology optimization, in which both scales are optimized simultaneously [68, 69].

5. References

[1] E. Gartner and H. Hirao. "A review of alternative approaches to the reduction of CO2 emissions associated with the manufacture of the binder phase in concrete". In: *Cement and Concrete Research* 78 (2015). Keynote papers from 14th International Congress on the Chemistry of Cement (ICCC 2015), pp. 126–142. DOI: 10.1016/j.cemconres.2015.04.012.

[2] K. L. Scrivener, V. M. John, and E. M. Gartner. "Eco-efficient cements: Potential economically viable solutions for a low-CO2 cement-based materials industry". In: *Cement and Concrete Research* 114 (Aug. 2018), pp. 2–26. DOI: 10.1016/j.cemconres.2018.03.015.

[3] P. Preinstorfer, B. Kromoser, and J. Kollegger. "Flexural behaviour of filigree slab elements made of carbon reinforced UHPC". In: *Construction and Building Materials* 199 (2019), pp. 416–423. DOI: 10.1016/j.conbuildmat.2018.12.027.

[4] T. Helbig et al. "Fuß- und Radwegbrücke aus Carbonbeton in Albstadt-Ebingen: Die weltweit erste ausschließlich carbonfaserbewehrte Betonbrücke". In: *Beton- und Stahlbetonbau* 111 (10 2016), pp. 676–685. DOI: 10.1002/best.201600058.

[5] L. Laiblová et al. "Environmental impact of textile reinforced concrete facades compared to conventional solutions-lca case study". In: *Materials* 12 (19 Aug. 2019). DOI: 10.3390/ma12193194.

[6] A. Jayasinghe et al. "Comparing different strategies of minimising embodied carbon in concrete floors". In: *Journal of Cleaner Production* 345 (Aug. 2022). DOI: 10.1016/j.jclepro.2022.131177.

[7] J. Hegger et al. "Load-bearing behaviour and simulation of textile reinforced concrete". In: *Materials and Structures/Materiaux et Constructions* 39 (8 2006), pp. 765–776. DOI: 10.1617/s11527-005-9039-y.

[8] Q. Yu et al. "A consistent safety format and design approach for brittle systems and application to textile reinforced concrete structures". In: *Engineering Structures* 249 (2021), p. 113306. DOI: 10.1016/j.engstruct.2021.113306.

[9] A. Fuchs, I. Curosu, and M. Kaliske. "Numerical Mesoscale Analysis of Textile Reinforced Concrete". In: *Materials* 13.18 (2020), p. 3944. DOI: 10.3390/ma13183944.

[10] N. W. Portal et al. "Numerical Modelling of Textile Reinforced Concrete". In: *Proceedings of the VIII International Conference on Fracture Mechanics of Concrete and Concrete Structures (FraMCoS-8)*. Ed. by J. G. M. van Mier et al. Toledo, Spain: FraMCoS Association, 2013.

[11] M. E. Kadi et al. "A layered-wise, composite modelling approach for fibre textile reinforced cementitious composites". In: *Cement and Concrete Composites* 94 (2018), pp. 107–115. DOI: 10.1016/j.cemconcomp.2018.08.015.

[12] R. Chudoba, E. Sharei, and A. Scholzen. "A strain-hardening microplane damage model for thin-walled textile-reinforced concrete shells, calibration procedure, and

experimental validation". In: *Composite Structures* 152 (2016), pp. 913–928. DOI: 10.1016/j.compstruct.2016.06.030.

[13] R. Chudoba et al. "Numerical Modeling of Non-Uniformly Reinforced Carbon Concrete Lightweight Ceiling Elements". In: *Applied Sciences* 9.11 (2019), p. 2348. DOI: 10.3390/app9112348.

[14] I. G. Lepenies. "Zur hierarchischen und simultanen Multi-Skalen-Analyse von Textilbeton". PhD thesis. 2007.

[15] J. Yvonnet. *Computational Homogenization of Heterogeneous Materials with Finite Elements*. Vol. 258. Springer International Publishing, 2019. DOI: 10.1007/978-3-030-18383-7.

[16] A. Sciegaj et al. "Upscaling of three-dimensional reinforced concrete representative volume elements to effective beam and plate models". In: *International Journal of Solids and Structures* 202 (2020), pp. 835–853. DOI: 10.1016/j.ijsolstr.2020.07.006.

[17] M. Richter. "Development of mechanical models for the analytical description of the material behaviour of textile reinforced concrete". PhD thesis. TU Dresden, 2005.

[18] B. Zastrau, I. G. Lepenies, and M. Richter. "On the Multi Scale Modeling of Textile Reinforced Concrete". In: *Technische Mechanik* 1 (2008), pp. 53–63.

[19] M. Huguet et al. "Stress resultant nonlinear constitutive model for cracked reinforced concrete panels". In: *Engineering Fracture Mechanics* 176 (May 2017), pp. 375–405. DOI: 10.1016/j.engfracmech.2017.02.027.

[20] J. Dornheim et al. "Neural Networks for Constitutive Modeling: From Universal Function Approximators to Advanced Models and the Integration of Physics". In: *Archives of Computational Methods in Engineering* 31.2 (2024), pp. 1097–1127. DOI: 10.1007/s11831-023-10009-y.

[21] I. B. C. M. Rocha, P. Kerfriden, and F. P. van der Meer. "On-the-fly construction of surrogate constitutive models for concurrent multiscale mechanical analysis through probabilistic machine learning". In: *Journal of Computational Physics: X* 9 (2021), p. 100083. DOI: 10.1016/j.jcpx.2020.100083.

[22] V. M. Nguyen-Thanh et al. "A surrogate model for computational homogenization of elastostatics at finite strain using high-dimensional model representation-based neural network". In: *International Journal for Numerical Methods in Engineering* 121.21 (2020), pp. 4811–4842. DOI: 10.1002/nme.6493.

[23] M. Vogler, R. Rolfes, and P. P. Camanho. "Modeling the Inelastic Deformation and Fracture of Polymer Composites – Part I: Plasticity Model". In: *Mechanics of Materials* 59 (2013), pp. 50–64. DOI: 10.1016/j.mechmat.2012.12.002.

[24] A. Sciegaj, F. Larsson, and K. Lundgren. "Experiments and Calibration of a Bond-Slip Relation and Efficiency Factors for Textile Reinforcement in Concrete". In: *Cement and Concrete Composites* 134 (2022), p. 104756. DOI: 10.1016/j.cemconcomp.2022.104756.

[25] A. Sciegaj et al. "Textile reinforced concrete members subjected to tension, bending, and in-plane loads: Experimental study and numerical analyses". In: *Construction and Building Materials* 408 (2023). DOI: 10.1016/j.conbuildmat.2023.133762.

[26] W. Brameshuber, ed. *Textile Reinforced Concrete: State-of-the-Art Report of RILEM TC 201-TRC*. Vol. 36. RILEM State-of-the-Art Reports. Bagneux, France: RILEM Publications SARL, 2006.

[27] C. Gielis et al. "3D Textile Reinforced Cement (TRC) composites with integrated synthetic microfibres: Evaluation of mechanical response and crack formation in bending". In: *Construction and Building Materials* 426 (2024), p. 136120. DOI: https://doi.org/10.1016/j.conbuildmat.2024.136120.

[28] J. Orlowsky, M. Beßling, and V. Kryzhanovskyi. "Prospects for the Use of Textile-Reinforced Concrete in Buildings and Structures Maintenance". In: *Buildings* 13 (1 2023). DOI: 10.3390/buildings13010189.

[29] RILEM TC 232-TDT. "Recommendation of RILEM TC 232-TDT: Test methods and design of textile reinforced concrete". In: *Materials and Structures* 49.12 (2016), pp. 4923–4927. DOI: 10.1617/s11527-016-0839-z.

[30] A. Peled, A. Bentur, and B. Mobasher. *Textile reinforced concrete.* CRC Press Inc, 2016.

[31] M. Konrad and R. Chudoba. "Tensile Behavior of Cementitious Composite Reinforced with Epoxy Impregnated Multifilament Yarns". In: *International Journal for Multiscale Computational Engineering* 7 (Jan. 2009), pp. 115–133. DOI: 10.1615/IntJMultCompEng.v7.i2.40.

[32] M. C. Rampini et al. "Mechanical behaviour of TRC composites: Experimental and analytical approaches". In: *Applied Sciences* 9 (7 2019). DOI: 10.3390/app9071492.

[33] J. Hegger and S. Voss. "Investigations on the bearing behaviour and application potential of textile reinforced concrete". In: *Engineering Structures* 30 (7 2008), pp. 2050–2056. DOI: 10.1016/j.engstruct.2008.01.006.

[34] J. U. Hartig. "Numerical investigations on the uniaxial tensile behaviour of Textile Reinforced Concrete Numerische Untersuchungen zum einaxialen Zugtragverhalten von Textilbeton". PhD thesis. Technische Universität Dresden, Aug. 2010.

[35] A. Hillerborg. *A Model for Fracture Analysis.* Tech. rep. Lund University, 1978.

[36] European Committee for Standardization (CEN). *Eurocode 2: Design of Concrete Structures – Part 1-1: General Rules and Rules for Buildings.* Standard EN 1992-1-1. Brussels: European Committee for Standardization, 2004.

[37] H. Read and G. Hegemier. "Strain softening of rock, soil and concrete — a review article". In: *Mechanics of Materials* 3.4 (1984), pp. 271–294. DOI: https://doi.org/10.1016/0167-6636(84)90028-0.

[38] G. Markeset and A. Hillerborg. "Softening of Concrete in Compression: Localization and Size Effects". In: *Cement and Concrete Research* 25.4 (1995), pp. 702–708. DOI: 10.1016/0008-8846(95)00059-L.

[39] P. Valeri, M. Fernández Ruiz, and A. Muttoni. "Tensile response of textile reinforced concrete". In: *Construction and Building Materials* 258 (2020), p. 119517. DOI: 10.1016/j.conbuildmat.2020.119517.

[40] B. Banholzer, T. Brockmann, and W. Brameshuber. "Material and bonding characteristics for dimensioning and modelling of textile reinforced concrete (TRC) elements". In: *Materials and Structures* 39 (2006), pp. 749–763. DOI: 10.1617/s11527-006-9140-x.

[41] N. W. Portal et al. “Pull-out of textile reinforcement in concrete”. In: *Construction and Building Materials* 71 (Aug. 2014), pp. 63–71. DOI: 10.1016/j.conbuildmat.2014.08.014.

[42] W. Hawkins et al. “An Analytical Failure Envelope for the Design of Textile Reinforced Concrete Shells”. In: *Structures* 15 (2018), pp. 56–65. DOI: 10.1016/j.istruc.2018.06.001.

[43] J. Lubliner et al. “A plastic-damage model for concrete”. In: *International Journal of Solids and Structures* 25.3 (1989), pp. 299–326. DOI: 10.1016/0020-7683(89)90050-4.

[44] P. Grassl and M. Jirásek. “Damage-plastic model for concrete failure”. In: *International Journal of Solids and Structures* 43.22 (2006), pp. 7166–7196. DOI: https://doi.org/10.1016/j.ijsolstr.2006.06.032.

[45] P. Grassl et al. “CDPM2: A damage-plasticity approach to modelling the failure of concrete”. In: *International Journal of Solids and Structures* 50.24 (2013), pp. 3805–3816. DOI: https://doi.org/10.1016/j.ijsolstr.2013.07.008.

[46] M. C. Rampini et al. “Stiffness Degradation of Textile-Reinforced Mortar under Unloading–Reloading Tensile Cycles”. In: *Journal of Composites for Construction* 27.1 (2023), p. 04022083. DOI: 10.1061/(ASCE)CC.1943-5614.0001273.

[47] J. Hartig, U. Häußler-Combe, and K. Schicktanz. “A Lattice Model Approach to the Uniaxial Behaviour of Textile Reinforced Concrete”. In: *Proceedings of the 6th International Conference on Fracture Mechanics of Concrete and Concrete Structures (FraMCoS-6)*. Ed. by A. Carpinteri et al. Catania, Italy: Taylor & Francis, 2007, pp. 745–752.

[48] J. Hartig, U. Häußler-Combe, and K. Schicktanz. “Influence of bond properties on the tensile behaviour of Textile Reinforced Concrete”. In: *Cement and Concrete Composites* 30.10 (2008), pp. 898–906. DOI: 10.1016/j.cemconcomp.2008.08.004.

[49] J. Mazars, F. Hamon, and S. Grange. “A new 3D damage model for concrete under monotonic, cyclic and dynamic loadings”. In: *Materials and structures* 48.11 (Nov. 2015), pp. 3779–3793. DOI: 10.1617/s11527-014-0439-8.

[50] C. Comi and U. Perego. “Fracture energy based bi-dissipative damage model for concrete”. In: *International Journal of Solids and Structures* 38.36–37 (2001), pp. 6427–6454. DOI: 10.1016/S0020-7683(01)00066-X.

[51] K. Matouš et al. “A review of predictive nonlinear theories for multiscale modeling of heterogeneous materials”. In: *Journal of Computational Physics* 330 (2017), pp. 192–220. DOI: 10.1016/j.jcp.2016.10.070.

[52] F. Feyel and J.-L. Chaboche. “FE2 multiscale approach for modelling the elasto-viscoplastic behaviour of long fibre SiC/Ti composite materials”. In: *Computer Methods in Applied Mechanics and Engineering* 183 (3 2000), pp. 309–330. DOI: https://doi.org/10.1016/S0045-7825(99)00224-8.

[53] S. Saeb, P. Steinmann, and A. Javili. “Aspects of Computational Homogenization at Finite Deformations: A Unifying Review From Reuss’ to Voigt’s Bound”. In: *Applied Mechanics Reviews* 68.5 (Sept. 2016), p. 050801. DOI: 10.1115/1.4034085.

[54] A. Bensoussan, J.-L. Lions, and G. Papanicolaou. *Asymptotic Analysis for Periodic Structures*. Amsterdam: North-Holland, 1978.

[55] M. G. D. Geers, V. G. Kouznetsova, and W. A. M. Brekelmans. "Multi-scale computational homogenization: Trends and challenges". In: *Journal of Computational and Applied Mathematics* 234 (7 2010), pp. 2175–2182. DOI: 10.1016/j.cam.2009.08.077.

[56] B. C. N. Mercatoris and T. J. Massart. "A coupled two-scale computational scheme for the failure of periodic quasi-brittle thin planar shells and its application to masonry". In: *International Journal for Numerical Methods in Engineering* 85 (2011), pp. 1177–1206. DOI: 10.1002/nme.3018.

[57] K. S. Challagulla et al. "Micromechanical analysis of grid-reinforced thin composite generally orthotropic shells". In: *Composites Part B: Engineering* 39 (2008), pp. 627–644. DOI: 10.1016/j.compositesb.2007.06.005.

[58] E. Börjesson et al. "Variationally consistent homogenisation of plates". In: *Computer Methods in Applied Mechanics and Engineering* 413 (2023). DOI: 10.1016/j.cma.2023.116094.

[59] E. W. C. Coenen, V. G. Kouznetsova, and M. G. D. Geers. "Computational homogenization for heterogeneous thin sheets". In: *International Journal for Numerical Methods in Engineering* 83 (8-9 2010), pp. 1180–1205. DOI: 10.1002/nme.2833.

[60] M. Petracca et al. "Multiscale computational first order homogenization of thick shells for the analysis of out-of-plane loaded masonry walls". In: *Computer Methods in Applied Mechanics and Engineering* 315 (2017), pp. 273–301. DOI: 10.1016/j.cma.2016.10.046.

[61] F. Larsson, K. Runesson, and F. Su. "Variationally consistent computational homogenization of transient heat flow". In: *International Journal for Numerical Methods in Engineering* 81 (13 Aug. 2010), pp. 1659–1686. DOI: 10.1002/nme.2747.

[62] M. G. D. Geers, V. G. Kouznetsova, and W. A. M. Brekelmans. "Multi-scale First-order and Second-order Computational Homogenization of Microstructures towards Continua". In: *International Journal for Multiscale Computational Engineering* 1.4 (2003), pp. 371–386. DOI: 10.1615/IntJMultCompEng.v1.i4.40.

[63] N. S. Ottosen and M. Ristinmaa. "Thermodynamic Framework for Constitutive Modeling". In: *The Mechanics of Constitutive Modeling*. Oxford: Elsevier, 2005, pp. 551–589. DOI: 10.1016/B978-008044606-6/50021-7.

[64] J. C. Simo and J. W. Ju. "Strain- and stress-based continuum damage models—I. Formulation". In: *International Journal of Solids and Structures* 23.7 (1987), pp. 821–840. DOI: 10.1016/0020-7683(87)90083-7.

[65] J. Mazars. "A Description of Micro- and Macroscale Damage of Concrete Structures". In: *Engineering Fracture Mechanics* 25 (6 1986), pp. 729–737.

[66] P. Koechlin and S. Potapov. "Global Constitutive Model for Reinforced Concrete Plates". In: *Journal of Engineering Mechanics* 133.3 (2007), pp. 257–266. DOI: 10.1061/(ASCE)0733-9399(2007)133:3(257).

[67] A. Sciegaj et al. "A multiscale model for reinforced concrete with macroscopic variation of reinforcement slip". In: *Computational Mechanics* 63.2 (2019), pp. 139–158. DOI: 10.1007/s00466-018-1588-3.

[68] A. Ferrer et al. "Two-scale topology optimization in computational material design: An integrated approach". In: *International Journal for Numerical Methods in Engineering* 114.3 (2018), pp. 232–254. DOI: 10.1002/nme.5742.

[69] P. W. Christensen and A. Klarbring. *An Introduction to Structural Optimization*. Vol. 153. Springer Netherlands, 2008. DOI: 10.1007/978-1-4020-8666-3.